One-dimensional solution for electron heating in an inductively coupled plasma discharge

N. S. Yoon, S. S. Kim, C. S. Chang, and Duk-In Choi
Department of Physics, Korea Advanced Institute of Science and Technology, Taejon 305-701, Korea
(Received 30 October 1995)

A one-dimensional analytic solution, which is valid for general collision frequencies and device lengths, has been obtained for plasma heating in a planar-type inductively coupled plasma (ICP) discharge. The analytic solution agrees with a particle simulation result based on the particle in cell method, and it indicates the existence of an optimum chamber length. An exact analytic solution for the surface impedance is obtained in the form of a series expansion. It is also shown that a simplified approximate form may be used for high-density ICP discharges.

PACS number(s): 52.80.Pi, 52.50.−b, 52.65.−y, 52.75.−d

I. INTRODUCTION

Inductively coupled plasma (ICP) sources have been the subject of many experimental and theoretical investigations [1–10] owing to the fact that a high-density plasma with good uniformity is easily obtained under low pressure without external magnetic field. Two types of ICP reactors are available [11], being classified according to the shape and the position of the coil. One type of reactor has a planar coil at the top of the cylindrical chamber (planar type) [1–9], and the other type has a solenoidal coil wound at the side of the chamber (solenoidal type) [10]. Both types of ICP reactors have many other attractive features such as the absence of electrode, low and controllable ion energies, etc. Moreover, an ICP reactor can be easily scaled up to accommodate a larger wafer size relative to the other reactors (Helicon, ECR, etc.) because the system is substantially simpler.

Usual understanding of the heating mechanism in radio frequency discharge relies on collisional dissipation of the wave energy. However, recent experimental results [1,3] in low-pressure ICP discharges indicate that the discharges cannot be understood without a collisionless electron heating mechanism. It has also been suggested, in both planar type [12] and solenoidal type [10], that the collisionless electron heating mechanism is a warm plasma effect analogous to the anomalous skin effect in metals. The anomalous skin effect is a transverse analog of the Landau damping in the standpoint of wave-particle interaction in plasma [13]. The electrons gain energy from the wave through the resonant coupling with the transverse electromagnetic waves.

The collisionless heating is now widely accepted to be the primary mechanism in sustaining low-pressure inductive radio frequency discharges. A general analytic representation of the plasma surface impedance is needed for a complete modeling of ICP plasmas [14]. An analytic formula [12,13,15] of surface impedance for half infinite plasma is available in some limiting cases only. Recent investigation by Ref. [12] indicates that a proper inclusion of finite chamber length is important and that an improved analytical approach is needed for such study. The anomalous skin effect in a bounded plasma has been studied in Refs. [16–19] with a symmetric wave and, thus, current source. However, their results are not applicable to a planar-type ICP discharge reactor because it has a wave and, thus, a current source at one side of the plasma boundary only. (There is a conducting boundary at the other side.) It is worth noting here that modulation of the wave electric field by a conducting boundary at the other side of the plasma strongly affects the electron heating mechanism when the chamber length L is not much greater than the plasma skin depth δ.

Lack of a general heating formula, which is valid for arbitrary chamber length and electron collisionality, has hindered an accurate modeling of the plasma discharge phenomena. A general description of the electron heating in an ICP discharge has been difficult to make because of the nonlocal property of the electron interaction with the wave. The random electron thermal motion is sufficiently large that the electrons experience strongly inhomogeneous wave oscillation during their collisionless spatial travel. Thus the electron heating at a reference point is a result of the inhomogeneous wave-particle interaction at different spatial points in the past. What makes the problem more complicated is the fact that most of the electrons bounce back at the material interface or plasma-vacuum port because of the sheath (or presheath) potential. Thus, the bounce motions constitute an important part of an electron's past history. If we take a typical loss speed of the plasma at the plasma-sheath boundary to be the ion sound speed v_s $(=\sqrt{T_e/M})$, the electrons bounce roughly $v_{\rm th}/v_s$ $(=\sqrt{M/m}\sim 500$ for argon discharge) times between the sheath boundaries before they escape from the electrostatic potential well. Here $v_{\rm th}$ $(=\sqrt{T_e/m})$ is the electron thermal velocity, and M and m are the mass of ions and electrons, respectively. Therefore, a perfectly reflecting boundary condition is a reasonable approximation for the electron reflection at the plasma boundaries.

We present an analytic, one-dimensional solution of the electron heating problem in terms of the well-known conductivity of the homogeneous hot plasma. The present solution is attempted for arbitrary values of δ/L and ν/ω in planar-type ICP discharges, where ν and ω are the electron elastic collision frequency with neutral atoms and angular wave frequency, respectively. The perfectly reflecting boundary condition is utilized to convert the finite sized nonlocal heating problem to a periodic system with infinite range. This equivalent infinite periodic system problem is then described by the conductivity of homogeneous plasma. The obtained solution is later compared with collisionless particle simula-

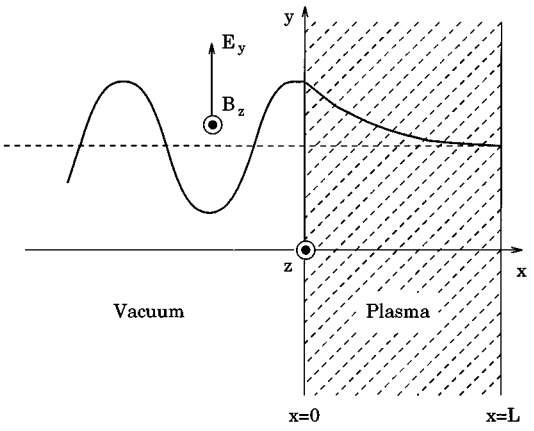

FIG. 1. Schematic diagram of wave propagation into a one-dimensional plasma.

tion results from the particle in cell (PIC) method [20] and the Langdon-Dawson advective algorithm [21] for the collisionless plasma ($\nu/\omega=0$).

Section II describes the derivation of a general analytic solution of electron heating, and Sec. III presents a method of numerical particle simulation. Section IV shows the comparison between the analytic and numerical results, and Sec. V contains concluding remarks for the present study.

II. DERIVATION OF ANALYTIC FORMULAS

A. Solution of a Maxwell-Boltzmann system

As can be seen from a schematic diagram in Fig. 1, plasma occupies spatial region $0\leqslant x\leqslant L$. A linearly polarized plane electromagnetic wave enters the plasma at $x=0$, and a conducting boundary exists at $x=L$. In the previous studies of symmetric systems [16–19], the wave entered through both boundaries $x=0$ and L. Thus, the present problem is considerably more difficult. For the electromagnetic field boundary conditions we take $B_z(0)=B_0$ and $E_y(L)=0$. The value of B_z at L, $B_z(L)$ ($\equiv B_L$) is determined by the condition $E_y(L)=0$.

If ion motion is neglected, using the time varying factor $\exp(-i\omega t)$ for all physical quantities, the current density J_y for a linear medium is given without loss of generality as [13]

$$J_y(x)=\int_0^L \Sigma(x,x')E_y(x')dx', \tag{1}$$

where $\Sigma(x,x')$ is the nonlocal conductivity of the bounded plasma. A direct calculation of $\Sigma(x,x')$ accounting for sharp plasma boundaries is possible from the linearized Boltzmann equation with the Krook model collision operator:

$$-i\omega f_1+v_x\frac{\partial f_1}{\partial x}+\frac{eE_y}{T_e}v_y f_0=-\nu f_1, \tag{2}$$

where f_0 is the equilibrium part, f_1 is the perturbed part of the distribution function, v_x is the x component of the electron velocity, and a Maxwellian velocity distribution may be used for f_0. Such a solution for $\Sigma(x,x')$ would be useful in solving Maxwell's equations in a symmetric system, as was done in Refs. [17] and [19]. However, the present system is not symmetric in x because of the presence of a source at one side of the boundary only. Hence the procedure of Refs. [17] and [19] is not applicable here, and we will not make a direct calculation of $\Sigma(x,x')$ from Eq. (2). As can be seen later, Eq. (2) will be used only to obtain the electrical conductivity for an infinite homogeneous plasma.

Maxwell's equations describing transverse electromagnetic field perturbations are

$$\frac{\partial E_y}{\partial x}=-i\kappa B_z, \tag{3}$$

$$\frac{\partial B_z}{\partial x}=-\frac{4\pi}{c}J_y+i\kappa E_y, \tag{4}$$

where $\kappa(=\omega/c)$ is the vacuum wave number. The displacement current term can be neglected for low ω values in the radio-frequency range.

In the limit $\nu/\omega\gg 1$, the concept of electrical conductivity becomes local $J_y(x)=\sigma_c E_y(x)$. Solution of Eqs. (1)–(4) is then easily obtained, leading to the well-known collisional conductivity $\sigma_c=\omega_p^2/[4\pi(\nu-i\omega)]$ and

$$E_y(x)=-i\frac{4\pi}{c}\frac{\kappa}{q}\frac{\exp[q(2L-x)]-\exp[qx]}{1+\exp[2qL]}B_0, \tag{5}$$

where

$$q=\frac{\omega_p}{c}[\sqrt{\phi(1+\phi)/2}-i\sqrt{\phi(1-\phi)/2}]$$

with

$$\phi\equiv(1+\nu^2/\omega^2)^{-2}. \tag{6}$$

Collisional surface impedance in its usual definition [22] then becomes

$$Z_s^{\rm coll}\equiv\left(\frac{4\pi}{c}\frac{E_y}{B_z}\right)_{x=0}=-i\frac{4\pi}{c}\frac{\kappa}{q}\tanh(qL). \tag{7}$$

In the present work we obtain an exact solution of Eqs. (1)–(4) for general collisionality, using the perfectly reflective boundary conditions. Let us consider all the possible contributions to the current density $J_y(x)$ at x by the electrons at x'. Their contributions can be classified into five different groups, depending on the way they reflect at the two boundaries (often called walls in this work):

$$\begin{aligned}J_y(x)=&\int_0^L\sigma(x-x')E_y(x')dx'+\sum_{n=0}^{\infty}\int_0^L\{\sigma(x+x'+2nL)\\&+\sigma[x+x'-2(n+1)L]+\sigma[x-x'-2(n+1)L]\\&+\sigma[x-x'+2(n+1)L]\}E_y(x')dx',\end{aligned} \tag{8}$$

where σ is the conductivity of the infinite homogeneous plasma. The first term represents direct contribution from the electrons at location x' without any reflection at the walls. The second (third) term represents contribution from the

electrons that initially start at x' toward the wall located at $x=0$ ($x=L$) and, after making n round trips bounce between the two walls and arrive at x from the wall at $x=0$ ($x=L$). The fourth (fifth) term represents the effects of electrons that initially start at x' toward the wall located at $x=0$ ($x=L$) and, after bouncing n times between the two walls, arrive at x from the wall at $x=L$ ($x=0$).

If we extend the definition of $E_y(x)$ into the domains $x<0$ and $x>L$ by the relationship

$$\begin{aligned} E_y(-x'-2nL) &\equiv E_y(x'), \\ E_y[-x'+2(n+1)L] &\equiv E_y(x'), \\ E_y[x'-2(n+1)L] &\equiv E_y(x'), \\ E_y[x'+2(n+1)L] &\equiv E_y(x') \quad (0\leqslant x'\leqslant L), \end{aligned} \tag{9}$$

the second term of Eq. (8) can be transformed into

$$\begin{aligned} &\sum_{n=0}^{\infty} \int_0^L \sigma(x+x'+2nL)E_y(x')dx' \\ &\quad = \int_0^L \sigma(x-x')E_y(x')dx' \\ &\qquad + \sum_{m=1}^{\infty} \int_{-L-2mL}^{-2mL} \sigma(x-x')E_y(x')dx', \end{aligned} \tag{10}$$

where the relations in Eq. (9) are used. If we transform the other terms similarly, Eq. (8) is transformed into a simple form,

$$\begin{aligned} J_y(x) &= \left[\int_{-L}^{L} + \sum_{m=1}^{\infty} \left\{ \int_{-L+2mL}^{L+2mL} + \int_{-L-2mL}^{L-2mL} \right\} \right] \\ &\quad \times \sigma(x-x')E_y(x')dx' \\ &= \int_{-\infty}^{\infty} \sigma(x-x')E_y(x')dx'. \end{aligned} \tag{11}$$

The current density $J_y(x)$ is now extended into an infinitely periodic system that is equivalent to the original finite system in the domain $0\leqslant x\leqslant L$ because the conductivity of infinite homogeneous plasma $\sigma(x)$ has the translational invariance [13]. The equivalent paths in this infinite periodic system S corresponding to the paths in the real system s are presented in Fig. 2.

If $x\neq x_n$, where $x_n=nL$ with an integer value n, Eqs. (1), (3), and (4) can be combined into a homogeneous wave equation,

$$\frac{\partial^2 E_y(x)}{\partial x^2} + \kappa^2 E_y = -\frac{4\pi\kappa}{c} i \int_{-\infty}^{\infty} \sigma(x-x')E_y(x')dx' \quad (x\neq x_n). \tag{12}$$

We will now obtain a solution of the homogeneous equation Eq. (12), with proper boundary conditions, by the Fourier transform method with the following Fourier series expansion:

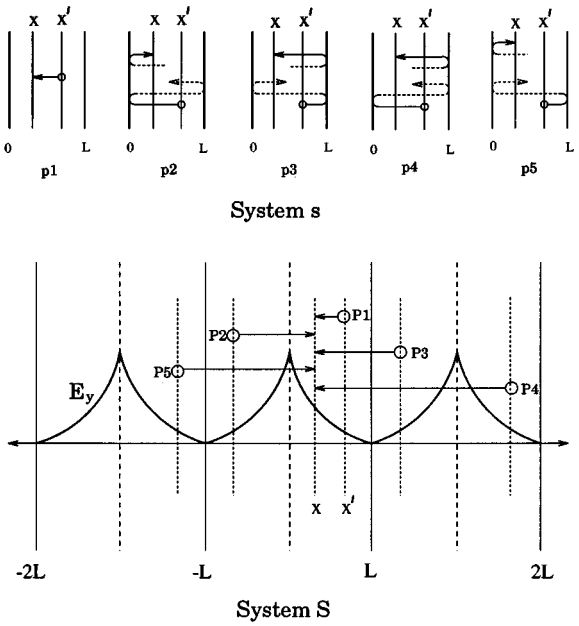

FIG. 2. Various probabilities of electron reflections and the equivalent paths in the infinite periodic system S corresponding to the paths in the real system s.

$$E(x) = \frac{e_0}{2} + \sum_{n=1}^{\infty} e_n \cos(q_n x), \quad q_n \equiv \frac{n\pi}{L}. \tag{13}$$

The Fourier series $E(x)$ in (13) and the real electric field $E_y(x)$ should be distinguished here. They have the same value at all points, but their derivatives are not equal at the boundaries. In a symmetric system as considered by the authors of Refs. [17] and [19], a Fourier solution was straightforward because of simple boundary conditions. In the present problem there is no simple form of the Fourier series that directly satisfies the asymmetric boundary conditions $B_z(0)=B_0$ and $B_z(L)=B_L$ [or $E_y(L)=0$]. In this work, we take an approach that is an extension of the method used in Ref. [13] for a half infinite plasma case.

It is important to notice here that the value of $\partial E(x)/\partial x$, as defined by Eq. (13), vanishes automatically at $x=x_n$, whereas the derivatives of the true electric field $E_y(x)$ at these points are not defined. In this extended periodic system, the gradient of the electric field (and thus the magnetic field itself) is not continuous at x_n. The discontinuity of the magnetic field can be resolved by a surface current density at $x=x_n$, and its value must be proportional to the difference between the right- and left-hand side values of the magnetic field. Since $B_z(x_n-0)=-B_z(x_n+0)$ in the periodic system, the surface current density needs to be equal to $2(c/4\pi)B_z(x_n+0)$ at each point $x=x_n$. Therefore the equivalent wave equation for $E(x)$ describing the infinitely periodic system becomes

$$\begin{aligned} \frac{\partial^2 E(x)}{\partial x^2} + \kappa^2 E &= -i\,\frac{4\pi}{c}\,\kappa \int_{-\infty}^{\infty} \sigma(x-x')E(x')dx' \\ &\quad + i\kappa \sum_{n=-\infty}^{\infty} B_z(x_n+0)\,\delta(x-x_n), \end{aligned} \tag{14}$$

where $\delta(x)$ is the Dirac delta function. The true finite system is then equivalent to the infinitely periodic system, which has proper surface currents at boundaries between the adjacent periodic systems. A particular solution of the inhomogeneous wave equation, Eq. (14), describing the infinite system, is equal to the solution of the homogeneous equation, Eq. (12), with the proper boundary conditions. Actually, in the true finite system the same solution is obtained whether B_0 and B_L are due to surface currents at the boundaries or some other current sources located at the exterior positions.

Although the conductivity of an infinite homogeneous plasma has a continuous wave-vector spectrum, the current density can be expanded by a discrete spectrum because the electric field is spatially periodic and thus has a discrete spectrum. The Fourier components of the current density are determined from a convolution of Eq. (11),

$$j_n \equiv \frac{1}{L}\int_{-L}^{L} J_y(x)\cos(q_n x)dx = \sqrt{2\pi}\,\sigma_{q_n} e_n, \qquad (15)$$

where σ_{q_n} is the Fourier component of the conductivity for an infinite homogeneous plasma, which is obtained from Eq. (2) by setting $\partial f_1/\partial x$ to zero,

$$\sigma_{q_n} \equiv \frac{1}{\sqrt{2\pi}}\int_{-\infty}^{\infty}\sigma(x)e^{-iq_n x}dx = \begin{cases} \dfrac{i}{\sqrt{\pi}}\dfrac{\omega_p}{8\pi}\,q_D\,\dfrac{v_{\rm th}}{\omega+i\nu} & (\text{if } q=0) \\ -\dfrac{i}{\sqrt{\pi}}\dfrac{\omega_p}{8\pi}\dfrac{q_D}{|q|}\,Z_p\!\left(\dfrac{\omega+i\nu}{|q_n|v_{\rm th}}\right) & (\text{otherwise}), \end{cases} \qquad (16)$$

where q_D is the Debye wave number defined by $q_D = \sqrt{4\pi n_e^2/T_e}$ and Z_p is the plasma dispersion function [23]. Now, a direct substitution of Eqs. (13) and (15) into Eq. (14) yields

$$e_n = -i\,\frac{2\kappa}{L}\,[B_0-(-1)^n B_L]Q_n, \qquad (17)$$

where the Q_n's are defined as

$$Q_n \equiv \left(q_n^2 - \frac{4\pi\omega}{c^2}\,i\sqrt{2\pi}\sigma_{q_n}\right)^{-1}. \qquad (18)$$

It can be easily checked that Eq. (17) recovers the symmetric result of Ref. [17] if we set $B_L = B_0$.

To complete the calculation, B_L needs to be determined from the boundary condition $E(L)=0$,

$$E(L)=0=\frac{e_0}{2}+\sum_{n=1}^{\infty}(-1)^n e_n = -i\,\frac{2\kappa}{L}\,(\Sigma_2 B_0 - \Sigma_1 B_L), \qquad (19)$$

which yields

$$B_L = \frac{\xi_2}{\xi}\,B_0, \qquad (20)$$

where

$$\xi_1 \equiv \frac{Q_0}{2}+\sum_{n=1}^{\infty}Q_n, \quad \xi_2 \equiv \frac{Q_0}{2}+\sum_{n=1}^{\infty}(-1)^n Q_n. \qquad (21)$$

Substituting (20) into Eq. (17), we obtain

$$e_n = -i\,\frac{2\kappa}{L}\,B_0[1-(-1)^n\xi_2/\xi_1]Q_n. \qquad (22)$$

The electric field $E_y(x)$ in the true system is then represented as

$$E_y(x)=E(x)=\frac{e_0}{2}+\sum_{n=1}^{\infty}e_n\cos(q_n x). \qquad (23)$$

The summation in (23) converges very rapidly with $Q_n \sim q_n^{-2} \sim n^{-2}$. Magnetic field $B_z(x)$ can be calculated from term-by-term differentiation of the Fourier series in $E(x)$ except at the points $x=(0 \text{ and } L)$, where the B_z values are given by the boundary condition and by (20), respectively:

$$B_z(x) = \begin{cases} B_0 & (x=0), \\ -\dfrac{i}{\kappa}\dfrac{\partial E(x)}{\partial x} = \dfrac{2B_0}{L}\displaystyle\sum_{n=1}^{\infty}[1-(-1)^n\xi_2/\xi_1]Q_n\sin(q_n x) & (0<x<L), \\ B_L = B_0\dfrac{\xi_2}{\xi_1} & (x=L). \end{cases} \qquad (24)$$

The Fourier sine series of B_z has a bad convergence near $x=(0 \text{ and } L)$ because $B_z(x)$ is not continuous at $x=(0 \text{ and } L)$ in the infinite periodic system, and thus an overshoot occurs at the discontinuities due to the well-known *Gibbs phenomena* [20]. Hence, a more careful treatment is necessary to obtain $B_z(x)$ near $x=(0 \text{ and } L)$. The convergence can be dramatically improved by using the following auxiliary functions:

$$b(x) \equiv b_0\left(1+\frac{B_L-B_0}{L}\,x\right), \qquad (25)$$

$$b_n = \frac{2}{L}\int_0^L \sin(q_n x)b(x)dx = \frac{2}{L}\,\frac{B_0}{q_n}\left(1-(-1)^n\,\frac{\xi_2}{\xi_1}\right),$$

$$\Delta(x) \equiv B_z(x) - b(x),$$

$$\Delta_n=\frac{2B_0}{L}\,(q_nQ_n-q_n^{-1})\left(1-(-1)^n\,\frac{\xi^2}{\xi_1}\right).$$

Here b_n and Δ_n are the coefficients of Fourier series $b(x)$ and $\Delta(x)$, respectively. We first calculate $\Delta(x)$ and then obtain $B_z(x)$ by adding $\Delta(x)$ to $b(x)$.

B. Surface impedance

With the above expressions for E_y and B_z, the surface impedance, defined as the coefficient of proportionality between $E_y(0)$ and $4\pi B_z(0)/c$, becomes

$$Z_s\equiv\frac{4\pi}{c}\,\frac{E_y(0)}{B_z(0)}=-i\kappa\,\frac{8\pi}{cL}\,\xi_1\left[1-\left(\frac{\xi_2}{\xi_1}\right)^2\right]. \tag{26}$$

Time-averaged power absorption per unit area is simply proportional to the real part of Z_s:

$$\frac{dP}{dt}=\frac{2}{8\pi}\,\mathrm{Re}[E_y(0)B_z^*(0)]=\frac{1}{2}\left(\frac{c}{4\pi}\right)^2\mathrm{Re}(Z_s)|B_0|^2. \tag{27}$$

However, in the present problem, since the effective surface current density becomes

$$K_{\mathrm{eff}}\equiv\int_0^L J_y(x)dx=\frac{c}{4\pi}\,(B_0-B_L), \tag{28}$$

the *impedance* Z_s does not obey Ohm's law and its imaginary part is not simply the inductance per unit length,

$$Z_s\neq\frac{E_y(0)}{K_{\mathrm{eff}}}, \tag{29}$$

$$\mathrm{Im}(Z_s)\neq\frac{\omega}{c}\,\mathrm{Re}\left(\frac{\Phi}{K_{\mathrm{eff}}}\right), \tag{30}$$

where Φ is magnetic flux per unit length. If the chamber length $L\to\infty$, and thus $|B_L|\to0$, the equalities in Eqs. (29) and (30) hold.

Equation (26) gives an exact general solution for electron heating in a planar-type inductively coupled plasma discharge with a perfectly reflecting boundary condition. The surface impedance Z_s is expressed in the form of series expansions, which converge rapidly as the number of terms increases.

To compare the present result with that of Refs. [12,13,15], we may take a short skin depth and long chamber length limit. In this limit a simple asymptotic expression of the surface impedance can be obtained by the method of complex integration used in Ref. [19]. The summations ξ_1 and ξ_2 can be written as

$$\begin{aligned}\xi_1&=\frac{lL}{2}\,S_1+\frac{v_{\mathrm{th}}c^2}{\omega\omega_p^2}\,(\omega+i\nu),\\ \xi_2&=\frac{lL}{2}\,S_2+\frac{v_{\mathrm{th}}c^2}{\omega\omega_p^2}\,(\omega+i\nu),\end{aligned} \tag{31}$$

where $l\equiv v_{\mathrm{th}}/\sqrt{\omega^2+\nu^2}$ and

$$S_1=\frac{2}{\rho}\sum_{n=1}^{\infty}\frac{1}{D(k_n)},\quad S_2=\frac{2}{\rho}\sum_{n=1}^{\infty}\frac{(-1)^n}{D(k_n)}, \tag{32}$$

with the following definitions for the additional quantities:

$$D(k_n)=k_n^2-\frac{\lambda}{k_n}\,Z_p\left(\frac{s}{k_n}\right),\quad \rho=\frac{L}{l},\quad k_n=q_nl,$$

$$s=\frac{\omega+i\nu}{\sqrt{\omega^2+\nu^2}},\quad \lambda=\frac{\omega\omega_p^2}{c^2}\,\frac{v_{\mathrm{th}}^2}{(\omega^2+\nu^2)^{3/2}}.$$

Here $1/\lambda$ can be interpreted as an anomalous skin depth.

If we use the relation $Z_p(\xi)+Z_p(-\xi)=2i\sqrt{\pi}e^{-\xi^2}$, the summations are rearranged as

$$S_1=S_1^{(1)}+S_1^{(2)},\quad S_2=S_2^{(1)}+S_2^{(2)}, \tag{33}$$

where

$$\begin{aligned}S_1^{(1)}&=\sum_{n=-\infty}^{\infty}{}'\,\frac{1}{\rho D(k_n)},\\ S_1^{(2)}&=2i\sqrt{\pi}\lambda\sum_{n=1}^{\infty}\frac{e^{-(s/k_n)^2}}{\rho k_nD(k_n)D(-k_n)},\end{aligned} \tag{34}$$

$$\begin{aligned}S_2^{(1)}&=\sum_{n=-\infty}^{\infty}{}'\,\frac{(-1)^n}{\rho D(k_n)},\\ S_2^{(2)}&=2i\sqrt{\pi}\lambda\sum_{n=1}^{\infty}\frac{(-1)^ne^{-(s/k_n)^2}}{\rho k_nD(k_n)D(-k_n)},\end{aligned} \tag{35}$$

and the notation Σ' denotes the summation over $n=0$. We extend the definition of k_n into the whole complex plane and consider the integrals

$$\int_\Gamma\frac{\cos(k\rho)}{D(k)\sin(k\rho)}\,dk,\quad \int_\Gamma\frac{1}{D(k)\sin(k\rho)}\,dk \tag{36}$$

along a path $\Gamma=\Gamma_1+\Gamma_2$, encircling all the roots η_m of the equation $D(k)=0$ and all the roots k_n of the equation $\sin(k\rho)=0$, excluding the origin $k=0$. Here the paths Γ_1 and Γ_2 are the same as those used in Ref. [19]. It can be shown that the point $k=0$ is an essential singularity, and the contour integral along a circle encircling the point $k=0$ vanishes as the radius of the circle goes to zero. Now, using the relations $\mathrm{Res}[\cot(k\rho);k_n]=1/\rho$ and $\mathrm{Res}[\csc(k\rho);k_n]=(-1)^n/\rho$, where $\mathrm{Res}[f(k);k_n]$ is the residue of $f(k)$ at $k=k_n$, we can represent the sums $S_1^{(1)}$ and $S_2^{(1)}$ as a sum of residues corresponding to the roots of the function $D(k)$:

$$\begin{aligned}S_1^{(1)}&=-\sum_{m=1}^{3}\cot(\eta_m\rho)\left/\frac{\partial D}{\partial k}\right|_{k=\eta_m},\\ S_2^{(1)}&=-\sum_{m=1}^{3}\csc(\eta_m\rho)\left/\frac{\partial D}{\partial k}\right|_{k=\eta_m}.\end{aligned} \tag{37}$$

When $\lambda\gg1$, the equation $D(k)=0$ has three roots:

$$\eta_m=\frac{1}{\alpha}\,e^{(\pi/2i+2m\pi i)/3}\left(1+\frac{i}{6}\,As\alpha e^{-(\pi/2i+2m\pi i)/3}\right)$$

$$(m=0,1,2), \quad (38)$$

where

$$\alpha=\pi^{-1/6}\lambda^{-1/3}, \quad A=\frac{4s}{\sqrt{\pi}}. \quad (39)$$

If Eq. (38) is substituted into Eq. (37), we have for sufficiently large ρ

$$S_1^{(1)}\cong\frac{2}{3}\,\alpha+\frac{As}{9}\,\alpha^2+\frac{4\lambda s}{9}\,\alpha^5, \quad (40)$$

$$S_2^{(1)}\cong-\frac{2\alpha}{3}\,(e^{(\eta_1\rho-2/3\pi)i}+e^{(\eta_2\rho+2/3\pi)i}+e^{(-\eta_3\rho+\pi/2)i}). \quad (41)$$

To derive Eq. (41), the following asymptotic expression for $\sin(k\rho)$ is used:

$$\sin(k\rho)\sim\begin{cases}-\dfrac{e^{-k\rho}}{2i} & (\mathrm{Im}\ k>0)\\ \dfrac{e^{ik\rho}}{2i} & (\mathrm{Im}\ k<0).\end{cases} \quad (42)$$

$S_2^{(1)}$ depends on $-|\mathrm{Im}\ \rho|$ exponentially, and thus the value of $S_2^{(1)}$ is negligible for large ρ.

The summation $S_1^{(2)}$ in Eq. (34) is equal to the integral

$$I_1=\frac{\lambda}{\sqrt{\pi}}\int_L\frac{e^{-(s/k)^2}}{kD(k)D(-k)}\cot(k\rho)dk, \quad (43)$$

where the path L surrounds the real axis in such a way that all zeros of the function $kD(k)D(-k)$ remain outside of this path, as in Ref. [19]. When ρ and λ are sufficiently large, the integral I_1 can be calculated approximately. Using the fact that the asymptotic value of $\cot(k\rho)$ has different signs for different signs of k [$\sim+i$ $(-i)$ when $\mathrm{Im}\ k_i<0$ (>0)], ρ is sufficiently large, the contour integral I_1 can be transformed into an integral along the real axis as

$$I_1=\frac{2i\lambda}{\sqrt{\pi}}\int_0^\infty\frac{e^{-(s/k)^2}}{kD(k)D(-k)}\,dk. \quad (44)$$

Developing the integrand of Eq. (44) into powers in α and taking the lowest order terms in α, we have

$$I_1\cong\frac{i\lambda}{\sqrt{\pi}}\,\alpha^4\int_0^\infty\frac{dt}{t^3+1+A\alpha t}=-\frac{i\lambda}{\sqrt{\pi}}\,\alpha^4\sum_{m=1}^{3}\frac{\ln t_m}{3t_m^2+A\alpha}, \quad (45)$$

where t_m is the three roots of the equation

$$t^3+1+A\alpha t=0. \quad (46)$$

Substituting the solutions of Eq. (46), up to the first order in α,

$$t_m=e^{(2m+1)\pi i/3}(1+A\alpha/3e^{(2m+1)\pi i/3}), \quad (47)$$

into Eq. (45), we find

$$S_1^{(2)}\cong2\sqrt{3}\,\frac{\pi i}{9}\,(1-A\alpha). \quad (48)$$

Combining Eqs. (40) and (48), S_1 becomes

$$S_1=\frac{2}{3\pi^{1/6}\lambda^{1/3}}\left(1+\frac{i}{\sqrt{3}}\right)+\frac{8s}{9\pi^{5/6}\lambda^{2/3}}\left(1-\frac{i}{\sqrt{3}}\right). \quad (49)$$

$S_2^{(2)}$ can be written as

$$S_2^{(2)}=I_2^{(1)}-I_2^{(2)}, \quad (50)$$

where

$$I_2^{(1)}=2i\sqrt{\pi}\lambda\sum_{n=1}^{\infty}\frac{e^{-(s/k_{2n})^2}}{\rho k_{2n}D(k_{2n})D(-k_{2n})},$$
$$I_2^{(2)}=2i\sqrt{\pi}\lambda\sum_{n=1}^{\infty}\frac{e^{-(s/k_{2n-1})^2}}{\rho k_{2n-1}D(k_{2n-1})D(-k_{2n-1})}. \quad (51)$$

Using $\mathrm{Res}[\cot(k\rho/2);k_{2n}]=2/\rho$ and $\mathrm{Res}[\tan(k\rho/2);k_{2n-1}]=-2/\rho$, we have

$$I_2^{(1)}=\frac{\lambda}{2\sqrt{\pi}}\int_L\frac{e^{-(s/k)^2}}{kD(k)D(-k)}\cot(k\rho)dk,$$
$$I_2^{(2)}=\frac{-\lambda}{2\sqrt{\pi}}\int_L\frac{e^{-(s/k)^2}}{kD(k)D(-k)}\tan(k\rho)dk. \quad (52)$$

Now the signs for the asymptotic values of $\cot(k\rho)$ and $\tan(k\rho)$ are opposite to each other. Therefore the asymptotic values of $I_2^{(1)}$ and $I_2^{(2)}$ are the same, and thus $S_2^{(2)}$ vanishes when ρ is sufficiently large.

From Eqs. (26), (31), and (49), and neglecting the second terms in Eq. (31), the final asymptotic expression for the surface impedance becomes

$$Z_s\cong Z_s^\infty=\frac{8\pi^{5/6}}{3}\left(\frac{1}{\sqrt{3}}-i\right)\left(\frac{\omega^2v_{\mathrm{th}}}{c^4\omega_p^2}\right)^{1/3}-\frac{32\pi^{1/6}}{9}\left(\frac{1}{\sqrt{3}+i}\right)$$
$$\times(\omega-i\nu)\left(\frac{\omega}{c^2\omega_p^4v_{\mathrm{th}}}\right)^{1/3} \quad \text{for } \lambda\gg1 \quad \text{and } \rho\gg1. \quad (53)$$

Z_s^∞ coincides with the asymptotic formula for half infinite plasma in Ref. [15]. The first term of Eq. (53) corresponds to the expression in Refs. [12] and [13], which was obtained by using a short wavelength limit of the plasma dispersion function with the value of $Z_p(|\omega/qv_{\mathrm{th}}|)\approx i\sqrt{\pi}$ and $\nu=0$. The validity of Eq. (53) for an actual ICP discharge condition can be put in doubt because if we take typical plasma parameters as $n_e=10^{12}$ cm^{-3}, $T_e=5$ eV, and $\omega=13.56$ MHz, the value of α is order of unity. However, as will be explained, we find that Eq. (53) can still be used for an approximate description of high-density ICP discharge.

III. NUMERICAL PARTICLE SIMULATION

A numerical particle simulation based on the particle in cell method [21,22,24] is performed to compare with the present analytic solution in the collisionless limit $\nu/\omega \ll 1$. The electron velocity distribution in v_x and v_y are given to be an isotropic Maxwellian at a constant temperature. Electrons can move freely along x with the velocity v_x. Whenever an electron collides with the walls during a time step, v_x changes sign and obeys the perfectly reflecting boundary condition. Ions are represented as uniform background charges, yielding the quasineutrality. Since the electrons move freely along x, a density fluctuation may exist. This density fluctuation is reduced by the self-consistent electrostatic field E_x.

To evaluate these effects, electrons are distributed by the particle distribution method, referred to as *quiet starts* in Refs. [21] and [25]. Spatial grid Δx is chosen to be about a Debye length in size [25], while the initial particle velocities are chosen from a random number generator (random starts). Although the particles have been placed initially to satisfy the charge neutrality in each cell, and thus there is no energy in the static field, some fluctuations of the E_x are generated as time advances. However, this fluctuating field energy is so small that the decrease of the electron temperature is negligible.

Maxwell's equations for the transverse fields in this model are

$$\frac{\partial E_y(x,t)}{\partial t} = -c\,\frac{\partial B_z(x,t)}{\partial x} - 4\pi J_y(x,t), \tag{54}$$

$$\frac{\partial B_z(x,t)}{\partial t} = -c\,\frac{\partial E_y(x,t)}{\partial x}. \tag{55}$$

These equations are solved by the Langdon-Dawson advective algorithm [22]. In this algorithm, the left- and right-going field quantities (^{-}F and ^{+}F) are defined as

$$^{\pm}F \equiv \tfrac{1}{2}(E_y \pm B_z). \tag{56}$$

By using grid spacing $\Delta z = c\Delta t$ and transforming Eqs. (54) and (55) into finite difference equations, the transverse field quantities at the kth grid point and nth time step become

$$^{\pm}F_k^{n+1} = {}^{\pm}F_{k\mp 1}^{n} - 2\pi J_{y,k\pm 1/2}^{n+1/2}\Delta t \quad (0 \leqslant k \leqslant K). \tag{57}$$

The Langdon differencing scheme of mesh current is adopted to calculate the current density at the $(k \pm 1/2)$th point and the $(n+1/2)$th time step as

$$J_{y,k\pm 1/2}^{n+1/2} = \sum_i q_i v_i^{n+1/2} \tfrac{1}{2}[S(X_{k\pm 1} - x_i^{n+1}) + S(X_k - x_i^n)], \tag{58}$$

where $S(x)$ is the particle shape factor. $S(x)$, corresponding to the first order interpolation scheme, can be written as

$$S(x) = \begin{cases} \dfrac{1}{\Delta x}\left(1 - \dfrac{x}{\Delta x}\right) & (0 \leqslant x \leqslant \Delta x) \\ \dfrac{1}{\Delta x}\left(1 + \dfrac{x}{\Delta x}\right) & (\Delta x \leqslant x \leqslant 0). \end{cases} \tag{59}$$

Since a particle has a finite size Δx in the PIC scheme, the simulated surface impedance is not for the point particles but for a particle cloud. The conductivity of the cloud in the Fourier space is

$$\sigma_q^{\text{cloud}} = \begin{cases} S^2(q)\,\dfrac{i}{\sqrt{\pi}}\,\dfrac{\omega_p}{8\pi}\,\dfrac{v_{\text{th}}}{\omega + i\nu} & (\text{if } q = 0) \\ -S^2(q)\,\dfrac{i}{\sqrt{\pi}}\,\dfrac{\omega_p}{8\pi}\,\dfrac{q_D}{|q|}\,Z_p\!\left(\dfrac{\omega + i\nu}{|q| v_t h}\right) & (\text{otherwise}), \end{cases} \tag{60}$$

where

$$S(q) = \int S(x) e^{-iqx} dx = \begin{cases} 1 & (\text{if } q = 0) \\ 2\,\dfrac{1 - \cos(q\Delta x)}{(q\Delta x)^2} & (\text{otherwise}). \end{cases} \tag{61}$$

The surface impedance of the electron cloud can be calculated by substituting σ_q in Eq. (18) by σ_q^{cloud}. It turns out that if we use the grid size Δx as small as the Debye length λ_D, the particle size effect becomes negligible. The reason why the effect is smaller for smaller Δx can be explained as follows: the value of $S(q)$ becomes small for $|q| \geqslant (\Delta x)^{-1}$, and thus the smaller the Δx is, the larger the number of modes to be included through $S(q)$ in Eq. (60). If Δx is sufficiently small, then $S(q)$ includes a sufficient number of modes to describe the physical phenomena for σ_q^{cloud} in Eq. (60).

Static field E_x is assumed to vanish at the boundaries [21], and the condition $E_y(L) = 0$ is taken as the right-hand side boundary condition of the field quantities. At the point $x = 0$, a value of the right-going field ^{+}F is given as the boundary condition. This boundary condition with $^{+}F(0)$, instead of $E_y(0)$ or $B_z(0)$, yields smoother profiles in the space- and time-dependent wave fields. Since $^{+}F(0)$ is the component of the right-going wave, this boundary condition is quite natural when there is a source at the left-hand side. In the real calculation, $^{+}F_k^{n+1}$ is computed from $k = 1$ K according to Eq. (57), $^{-}F_K^{n+1}$ is determined by $^{-}F_K^{n+1} = -{}^{+}F_K^{n+1}$, and finally the value of $^{-}F_k^{n+1}$ is found by decreasing the k values from $k = K - 1$ to 0 according to Eq. (57).

IV. COMPARISON OF ANALYTIC AND NUMERICAL RESULTS

The analytic and particle simulation results are compared by cross-checking various quantities such as the electric field $E_y(x)$, the magnetic field $B_z(x)$, the mean particle velocity $V_y(x)$, and the absorbed power density $J_y(x)E_y(x)$ at four different times in the rf period in Fig. 3. All quantities show good agreement. The electric and magnetic fields in the simulation results are very smooth spatially, while the transverse particle speed and power densities have some fluctuations. Although there are some fluctuations of $V_y(x)$, which cannot be avoided in a particle simulation, the influence of this fluctuation on the surface impedance is small because spatial and temporal profiles of the electric and the magnetic fields are very smooth. The spatial smoothness of the field quantities is due to the property of Eq. (57) and the use of

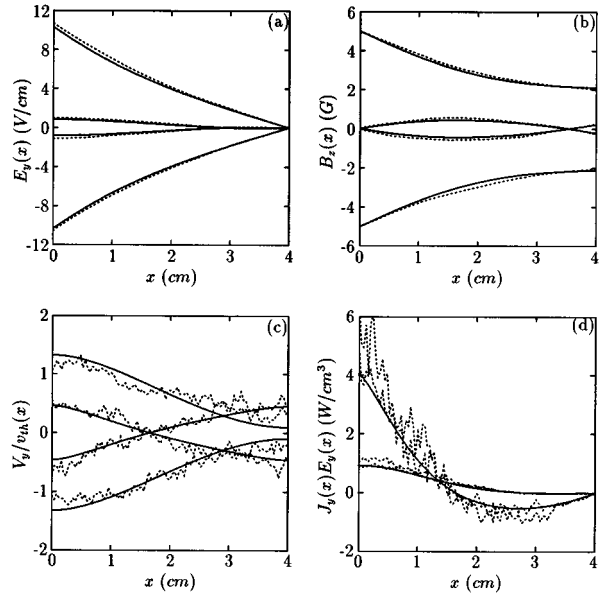

FIG. 3. Comparison between the analytic and the simulation results of various quantities at four different times 0, 1/4T, 2/4T, and 3/4T in a rf period T. Solid lines represent the analytic results and dotted lines represent particle simulation results. $n_e=10^{11}$ cm^{-3}, $T_e=5$ eV, and $\omega=13.56$ MHz are used.

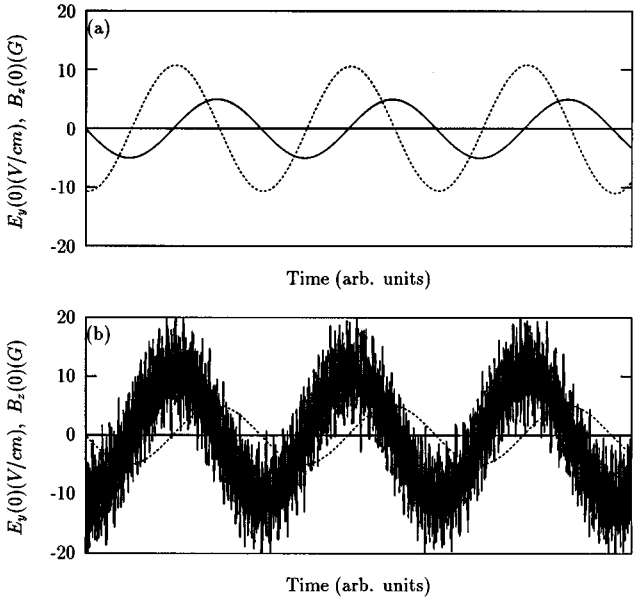

FIG. 4. $E_y(0)$ and $B_z(0)$ as functions of time obtained from the numerical particle simulation: (a) When $^{+}F(0)$ is given as the boundary condition, both $E_y(0)$ and $B_z(0)$ are smooth. (b) When $B_z(0)$ is given as the boundary condition, $E_y(0)$ shows fluctuation.

$^{+}F(0)$ as the boundary conditions rather than $E_y(0)$. The random fluctuations of J_y are averaged out during the successive calculations of $^{\pm}F_k$. If $E_y(0)$ is taken to be the boundary condition, it is observed that a wave packet is generated and it never damps out.

Temporal profiles of the electric and magnetic fields are very smooth also when $^{+}F(0)$ is used as the boundary condition, whereas they show significant level of fluctuations when $B_z(0)$ is used as the boundary condition (Fig. 4). The smooth time evolution of the electromagnetic fields indicates a good accuracy of the calculation of the surface impedance in the numerical simulation. The greater the $^{+}F(0)$ values are, the worse the temporal smoothness of the electric field becomes. This is because of the fact that at a stronger electromagnetic field strength, a nonlinear effect appears in the simulation, whereas the analytic results were obtained through the linearized Boltzmann equation. Under typical ICP operational conditions as reported in Refs. [1] and [2], a linear approximation is valid.

The analytic and simulation results of the surface impedance are compared in Fig. 5, showing good agreement in the collisionless limit $\nu/\omega \ll 1$. The agreement in the imaginary part is better than the real part. This is because the real and imaginary parts are proportional to cosine and sine components, respectively, of the phase difference ϕ between $E_y(0)$ and $B_z(0)$. Since ϕ is about $\pi/2$, the real part is more sensitive to the phase fluctuation of the electric and magnetic fields. This introduces greater numerical uncertainty in the simulation of the real part than in the imaginary part. In the other collisionality limit $\nu/\omega \gg 1$, there is no need to check the accuracy of the present analytic solution by numerical simulation because the usual analytic solution is easily found to agree well with the present analytic solution.

The real and imaginary parts of the surface impedance as a function of the chamber length in the limit $\nu/\omega \ll 1$ are presented in Figs. 6 and 7 with various electron densities. Since the value of Q_n is rapidly decreasing with increasing n, finite sums of N terms can be used:

$$\sum_{n=1}^{\infty} Q_n \cong \sum_{n=1}^{N} Q_n, \quad \sum_{n=1}^{\infty} (-1)^n Q_n \cong \sum_{n=1}^{N} (-1)^n Q_n. \tag{62}$$

An acceptable value of N depends on the chamber length L and the plasma parameters. For greater chamber length L, the larger value of N is required. The real part converges more rapidly than the imaginary part, in general. Since the absorbed power is proportional to the real part of the surface impedance, the peak in $\mathrm{Re}(Z_s)$ indicates the existence of an optimum chamber length.

The maximum surface impedance is due to the resonant coupling between the wave and the electron bounce motions. Two types of resonances are possible in a bounded plasma,

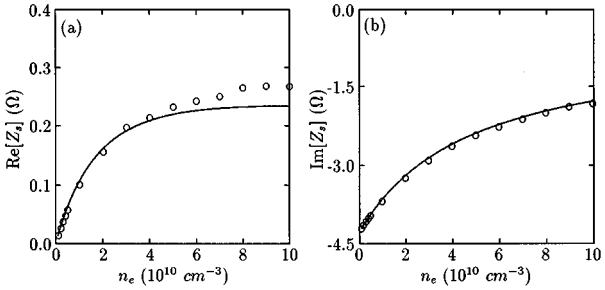

FIG. 5. Comparison between the analytic and particle simulation results for the surface impedance Z_s. Solid lines show the analytic results, and circles represent the simulation results. The simulation conditions, except n_e, are the same as those in Fig. 3.

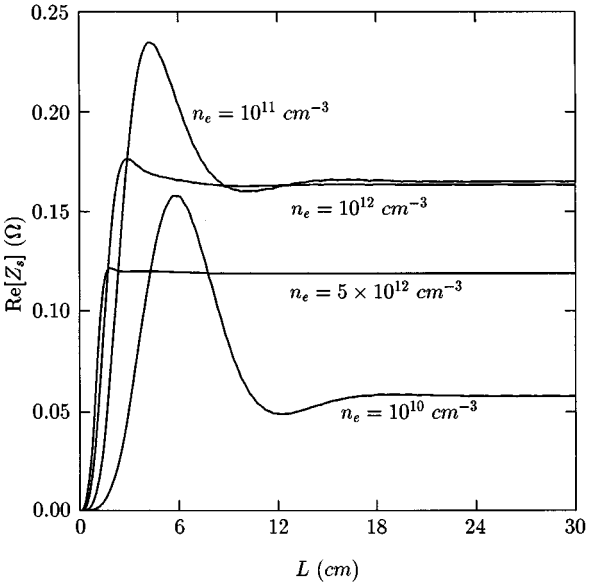

FIG. 6. Dependence of Re(Z_s) on L for various electron densities (T_e=5 eV and ν=0).

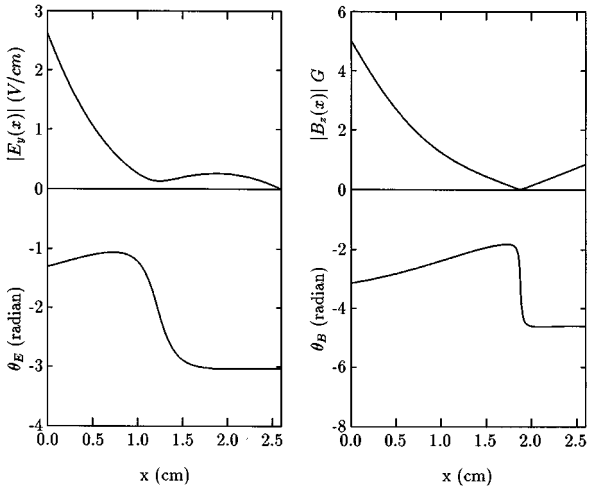

FIG. 8. Spatial variation of the amplitude and phase of the electric and the magnetic fields near the resonance. B_0=5 G, $n_e=10^{12}$ cm^{-3}, T_e=5 eV, and ν=0 are used.

as demonstrated in Ref. [17]. The first type occurs when the electrons traverse the chamber length L in a time equal to a multiple of the wave half period. This type of resonance is not related to the electron density.

The second type of resonance occurs when the electrons traverse a skin depth in a time equal to an odd multiple of the wave half period. The resonance conditions are

$$\frac{L/v_{\rm th}}{\tau/2}=1,2,3,\ldots \quad (\text{first type}), \tag{63}$$

$$\frac{\delta_s/v_{\rm th}}{\tau/2}=1,3,5,\ldots \quad (\text{second type}), \tag{64}$$

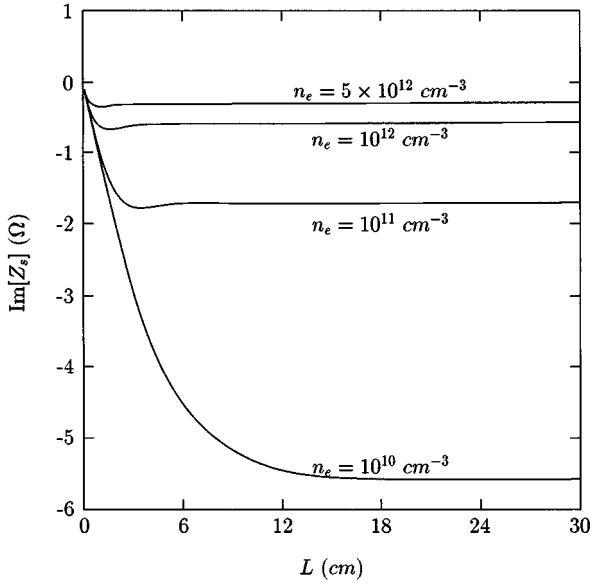

FIG. 7. Dependence of Im(Z_s) on L for various electron densities (T_e=5 eV and ν=0).

respectively, and the skin depth δ_s is defined by

$$\delta_s \equiv -\frac{2dx}{d\ \ln|E|^2}=-\frac{c}{4\pi\kappa}\frac{|Z_s|^2}{\mathrm{Im}[Z_s]}. \tag{65}$$

Since δ_s is always less than L, only the following cases can occur:

$$\text{case I:}\quad \frac{\delta_s/v_{\rm th}}{\tau/2}>1, \tag{66}$$

$$\text{case II:}\quad \frac{\delta_s/v_{\rm th}}{\tau/2}\leqslant 1 \quad \text{and} \quad \frac{L/v_{\rm th}}{\tau/2}\geqslant 1, \tag{67}$$

$$\text{case III:}\quad \frac{L/v_{\rm th}}{\tau/2}<1, \tag{68}$$

where $\tau=\pi/\omega$ is the half period of the wave. In case I, corresponding to low density or temperature, both types of resonances can occur. Only the first type of resonance can occur in case II, and there is no resonance in case III. The maximum value in the real part of the surface impedance is achieved in case II, as the chamber length matches the value of $\tau v_{\rm th}/2$. In case I the second peak in the real part of the surface impedance also appears at the device length about where the second type of resonance condition is satisfied (three halves of a wave period).

When the chamber length is near the optimum value, at which the real part of the surface impedance is maximum, the amplitude and phase of the magnetic fields have similar spatial profiles with the results reported in Ref. [17]. $|B_z(x)|$ shows a minimum at an x value. At the minimum x position, an abrupt phase change of $\sim\pm\pi$ in the magnetic field occurs

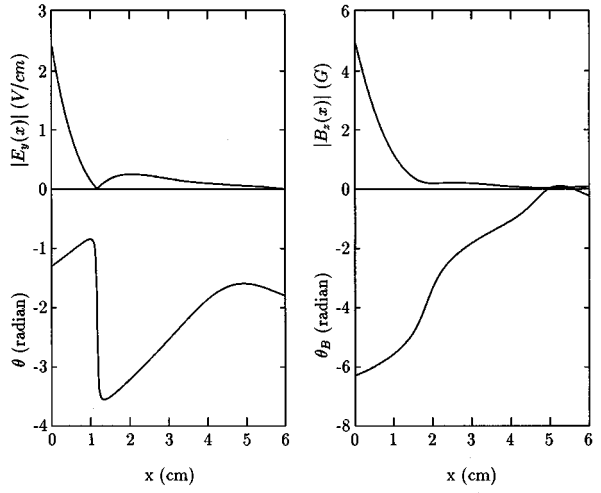

FIG. 9. Spatial variation of the amplitude and phase of the electric and magnetic fields when the chamber length is greater than the optimum length. All the conditions are the same as those in Fig. 6 except the chamber length L.

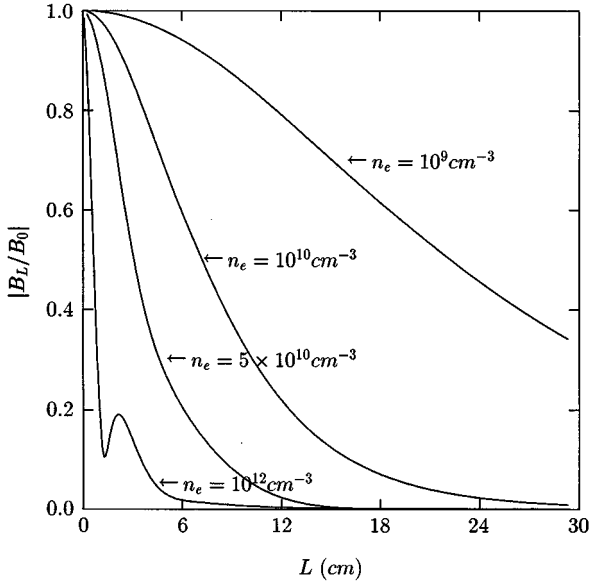

FIG. 11. Dependence of $|B_L/B_0|$ on L for various electron densities ($T_e=5$ eV and $\nu=0$).

(Fig. 8). However, if the chamber length is sufficiently longer than the optimum value, this phenomenon occurs in the electric field amplitude ($|E_y(x)|$) and phase (θ_E) rather than in the magnetic field (Fig. 9). The occurrence of a minimum of E_y is more pronounced at higher densities, and in this case the position of the minimum point does not depend on the chamber length. It is observed that the collisionality weakens the occurrence of the minimum phenomena. When the chamber length is smaller than the optimum length, there is no extreme point. Instead, the amplitudes of the field vectors are monotonically decreased.

The asymptotic formula Z_s^{∞} in Eq. (53) is compared with the exact formula Z_s in Eq. (26). Besides the fact that Z_s^{∞} yields unphysical negative values when the density is too small, it is seen that Z_s^{∞} is a good approximation for the steady state ICP-discharge conditions reported in Ref. [2]. Figure 10 shows a collisionless case ($\nu=0$) when $T_e=5$ eV and $L=5$ cm. It can be seen that we have a reasonably good agreement for $n_e > 1.5\times 10^{11}$ cm^{-3}. This good agreement between Z_s^{∞} and Z_s is surprising because under the condition of Fig. 10, the value of α is less than 2 and δ_s/L is not so small,

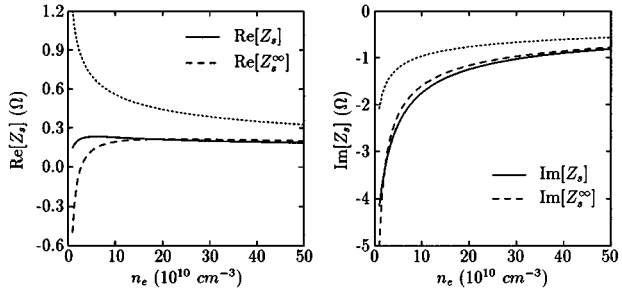

FIG. 10. Comparison of the asymptotic surface impedance Z_s^{∞} with Z_s. $T_e=5$ eV, $\nu=0$, and $L=5$ cm. Dotted lines represent the first term of Eq. (53).

weakening the simplifying assumptions. The dotted line represents the first term of Eq. (53), which corresponds to the results of Refs. [12] and [13]. Thus, we find that the results of Refs. [12] and [13] are too rough to be applied to planar-type ICP discharge. On the other hand, the result of Ref. [15], which obtained Z_s^{∞} of Eq. (53), can be used for an approximate description of a high-density ICP discharge. We find that Z_s agrees better with Z_s^{col} as the collision frequency is increased ($\nu/\omega \gg 1$).

The ratio $|B_L/B_0|$ is presented in Fig. 11. We can see that a local maximum appears when the density is high. This peak is related to the peak of the skin depth δ_s defined by Eq. (65). Since the amplitude of the electric field is not monotonic at high density, the skin depth has a maximum at a chamber length smaller than the optimal length; hence the increase of damping rate is not monotonic with increasing chamber length.

V. CONCLUSIONS

A one-dimensional analytic solution of the electron heating problem is obtained for arbitrary values of the chamber length and collision frequency in an inductively coupled plasma discharge with planar coil geometry. The analytic results of Eq. (26) agree with PIC simulation results. The present formulas show the existence of an optimum chamber length at which the coupling efficiency is maximum. An asymptotic formula for surface impedance, Eq. (53), is obtained by a complex integration method, and it coincides with the earlier formula for half infinite plasma [15]. It is shown here that the asymptotic form of the surface impedance is a reasonable approximation for a high-density steady state plasma in planar-type ICP discharge. The present results can easily be used in the future simulations of radio frequency planar ICP discharges. For a more exact description of electron heating for general plasma density, device length,

and collisionality, Eq. (26) may be used, which is expressed in the form of a series expansion. Since the series converges rapidly, a reasonable number (~ 10) of terms can be chosen to get a desired accuracy of practical value. For an even simpler description of the electron heating problem, the approximate formula of Eq. (53) may be used if the plasma density is reasonably high ($>0.5\times10^{11}$ cm^{-3}). The weakness of Eq. (53) lies in the fact that when the collisionality is low (ν/ω), Eq. (53) widely deviates from the real values if the plasma density is low ($<0.5\times10^{11}$ cm^{-3}).

The present one-dimensional treatment is expected to yield an error of order δ_s/R, which is usually a small quantity. Here R is the radius of the cylindrical ICP chamber. For a more accurate calculation of the electron heating to higher order in δ_s/R, a two-dimensional analysis may be considered in the future. This is under active study and will be reported later.

ACKNOWLEDGMENT

This work was supported by the Republic of Korea's Electronics and Telecommunications Research Institute (ETRI).

[1] J. Hopwood, C. R. Guarnier, S. J. Whitehair, and J. J. Cuomo, J. Vac. Sci. Technol. A **11**, 152 (1993).
[2] J. Hopwood, C. R. Guarnier, S. J. Whitehair, and J. J. Cuomo, J. Vac. Sci. Technol. A **11**, 147 (1993).
[3] J. H. Keller, J. C. Forster, and M. S. Barnes, J. Vac. Sci. Technol. A **11**, 2487 (1993).
[4] T. Fukasawa, T. Nouda, A. Nakamura, H. Shindo, and Y. Horike, Jpn. J. Appl. Phys. **32**, 6076 (1993).
[5] P. L. G. Ventzek, T. J. Sommerer, R. J. Hoekstra, and M. J. Kushner, J. Vac. Sci. Technol. B **12**, 461 (1994).
[6] P. L. G. Ventzek, R. J. Hekstra, and M. J. Kushner, J. Vac. Sci. Technol. B **12**, 461 (1994).
[7] R. A. Stewart, P. Vitello, and D. B. Graves, J. Vac. Sci. Technol. B **12**, 478 (1994).
[8] A. P. Paranjpe, J. Vac. Sci. Technol. A **12**, 2487 (1994).
[9] G. DiPeso, V. Vahedi, D. W. Hewett, and T. D. Rognlien, J. Vac. Sci. Technol. A **12**, 2487 (1994).
[10] R. B. Piejak, V. A. Godyak, and B. M. Alexandrovich, Plasma Sources Sci. Technol. **3**, 169 (1994).
[11] D. B. Graves, IEEE Trans. Plasma Sci. **22**, 1 (1994).
[12] M. M. Turner, Phys. Rev. Lett. **71**, 1844 (1993).
[13] S. Ichimaru, *Basic Principles of Plasma Physics: A Statistical Approach*, Frontiers in Physics (Benjamin, Reading, MA, 1973), Vol. 41.
[14] M. A. Lieberman and A. J. Lichtenberg, *Principles of Plasma Discharges and Materials Processing* (Wiley, New York, 1994).
[15] E. S. Weibel, Phys. Fluids **10**, 741 (1967).
[16] J. A. Reynolds, H. A. Blevin, and P. C. Thonemann, Phys. Rev. Lett. **22**, 762 (1969).
[17] H. A. Blevin, J. A. Reynolds, and P. C. Thonemann, Phys. Fluids **13**, 1259 (1970).
[18] H. A. Blevin, J. A. Reynolds, and P. C. Thonemann, Phys. Fluids **16**, 82 (1973).
[19] Y. S. Sayasov, Helv. Phys. Acta **52**, 288 (1979).
[20] C. K. Birdsall and A. B. Langdon, *Plasma Physics via Computer Simulation* (McGraw-Hill, Singapore, 1985).
[21] B. B. Godfrey and A. B. Langdon, J. Comput. Phys. **20**, 251 (1976).
[22] J. D. Jackson, *Classical Electrodynamics* (Wiley, New York, 1975).
[23] B. D. Fried and S. D. Conte, *The Plasma Dispersion Function* (Academic, New York, 1961).
[24] R. W. Hockney and J. W. Eastwood, *Computer Simulation Using Particles* (Hilger, Bristol, England, 1988).
[25] J. M. Dawson, Rev. Mod. Phys. **55**, 403 (1983).